

Microscopic Theory of Rashba Interaction in Magnetic Metal

Jin-Hong Park

*Department of Physics and BK21 Physics Research Division,
Sungkyunkwan University, Suwon 440-746, Korea*

Choong H. Kim

Department of Physics and Astronomy, Seoul National University, Seoul 151-742, Korea

Hyun-Woo Lee*

PCTP and Department of Physics, Pohang University of Science and Technology, Pohang, 790-784, Korea

Jung Hoon Han†

*Department of Physics and BK21 Physics Research Division,
Sungkyunkwan University, Suwon 440-746, Korea and
Asia Pacific Center for Theoretical Physics, POSTECH, Pohang, Gyeongbuk 790-784, Korea
(Dated: May 25, 2018)*

Theory of Rashba spin-orbit coupling in magnetic metals is worked out from microscopic Hamiltonian describing d -orbitals. When structural inversion symmetry is broken, electron hopping between d -orbitals generates chiral ordering of orbital angular momentum, which combines with atomic spin-orbit coupling to result in the Rashba interaction. Rashba parameter characterizing the interaction is band-specific, even reversing its sign from band to band. Large enhancement of the Rashba parameter found in recent experiments is attributed to the orbital mixing of $3d$ magnetic atoms with non-magnetic heavy elements as we demonstrate by first-principles and tight-binding calculations.

PACS numbers: 75.60.Jk

Control of the local magnetization direction in a metallic ferromagnet through delivery of torque by the current-carrying electrons is one of the major endeavors of spintronics community nowadays [1]. Prompted by the theoretical discovery of a new type of spin transfer torque (STT) arising in Rashba-coupled bands [2–5] and subsequent experimental indication thereof [6], several proposals [7, 8] were made recently to uncover a complete set of STT's permissible in ferromagnets with the Rashba-coupled bands, or Rashba ferromagnets for short. Experiments to measure Rashba-induced STT were performed for a very thin atomic layer of magnetic atoms with several layers of heavy atoms such as Pt grown on top [6]. It was predicted that the Rashba interaction can make the electric control of the magnetization dynamics drastically more efficient [8] and give rise to giant spin motive force [9], greatly raising the technological prospect of spintronic devices based on unprecedented strong mutual coupling of magnetization dynamics and electric current.

Compared to other spintronic phenomena such as giant magnetoresistance and spin Hall effect [10, 11], theories of the Rashba interaction in ferromagnets are largely phenomenological [2–4, 7–9], based on free electron-like Hamiltonian such as

$$\mathcal{H} = \mathcal{H}_0 + \mathcal{H}_{\text{ex}} + \mathcal{H}_{\text{R}}, \quad (1)$$

where $\mathcal{H}_0 = \mathbf{p}^2/2m$ gives the dynamics of conduction electrons in the parabolic approximation, $\mathcal{H}_{\text{ex}} = -J\boldsymbol{\sigma} \cdot \mathbf{n}$ is the ferromagnetic exchange coupling between the conduction electron spin $\boldsymbol{\sigma}$ and the localized moment \mathbf{n} , and

$\mathcal{H}_{\text{R}} = \alpha_{\text{R}}(\boldsymbol{\sigma} \times \mathbf{p}) \cdot \hat{z}$ is the Rashba spin-orbit coupling interaction, with the surface normal to a Rashba ferromagnet taken as the \hat{z} -axis. In these theories the Rashba parameter α_{R} is a purely phenomenological parameter, and it remains unclear what controls the strength of α_{R} . A naive estimation of α_{R} based on the relativistic effective magnetic field in free electron picture and consequent Zeeman energy results in $\sim 10^{-4}$ eVÅ, which is several orders of magnitude smaller than experimental values [6, 12, 13]. In light of the technological prospect of Rashba ferromagnets, not to mention the theoretical importance of the problem itself, we try to establish the Rashba interaction in ferromagnets on a microscopic level. In recent papers some of the present authors showed that the Rashba interaction in non-magnetic bands is essentially a multi-orbital phenomenon [14, 15]. A similar idea was proposed earlier in Ref. [16]. As the magnetically polarized bands also typically exhibit multi-orbital character with most of the d -orbitals involved in the band structure, the multi-orbital scheme may be brought to bear on the magnetic system as well.

Construction of a microscopic Hamiltonian is done for t_{2g} d -orbitals (d_{xy}, d_{xz}, d_{zx}) where magnetism typically occurs. We assume a square lattice and introduce the tight-binding Hamiltonian $H_{t_{2g}}$ for electron hopping to nearest neighbor sites with Slater-Koster parameters t_1 and t_2 for σ - and π -hopping of the d -orbitals. The inversion symmetry breaking (ISB) about the xy -plane gener-

ates additional hopping terms [17],

$$H_{\text{ISB}} = \gamma \sum_{i,\sigma} [c_{i,xy,\sigma}^\dagger c_{i+\hat{y},zx,\sigma} + c_{i,xy,\sigma}^\dagger c_{i+\hat{x},yz,\sigma} + h.c.] - \gamma \sum_{i,\sigma} [c_{i,xy,\sigma}^\dagger c_{i-\hat{y},zx,\sigma} + c_{i,xy,\sigma}^\dagger c_{i-\hat{x},yz,\sigma} + h.c.], \quad (2)$$

dictated by the ISB parameter γ . Here i denotes the atomic site and $c_{i,xy/yz/zx,\sigma}$ is the electron annihilation operator of the $d_{xy}/d_{yz}/d_{zx}$ orbital with the spin z -component σ . In addition, magnetic exchange H_{ex} and atomic spin-orbit interaction (SOI) Hamiltonian H_{SOI} are introduced as

$$H_{\text{ex}} = -J \sum_{i,\sigma,\sigma'} \mathbf{C}_{i,\sigma}^\dagger \mathbf{n} \cdot (\boldsymbol{\sigma})_{\sigma,\sigma'} \mathbf{C}_{i,\sigma'},$$

$$H_{\text{SOI}} = \lambda_{\text{so}} \sum_{i,\sigma,\sigma'} \mathbf{C}_{i,\sigma}^\dagger \mathbf{L} \cdot (\boldsymbol{\sigma})_{\sigma,\sigma'} \mathbf{C}_{i,\sigma'}, \quad (3)$$

where $\mathbf{C}_{i,\sigma}^\dagger = (c_{i,xy,\sigma}^\dagger, c_{i,yz,\sigma}^\dagger, c_{i,zx,\sigma}^\dagger)$, and \mathbf{L} is the 3×3 matrix consisting of the expectation values of the atomic orbital angular momentum (OAM) within the t_{2g} orbital space. This completes the microscopic model we shall study now: $H_{\text{TB}} = H_{t_{2g}} + H_{\text{ISB}} + H_{\text{ex}} + H_{\text{SOI}}$ [18].

Numerically determined energy bands of H_{TB} are shown in Fig. 1. The result indicates interesting dependence of the band dispersion on the relative direction of \mathbf{n} with respect to the Bloch momentum \mathbf{k} . When \mathbf{n} is either parallel or anti-parallel to \mathbf{k} we do not find any changes in the dispersion [Fig. 1(b)]. On the other hand, when \mathbf{n} is orthogonal to \mathbf{k} , a clear displacement of the band is observed [Fig. 1(a)] in the opposite directions according to whether $\mathbf{n} \parallel +\hat{z} \times \mathbf{k}$ or $\mathbf{n} \parallel -\hat{z} \times \mathbf{k}$. The amount of the displacement grows linearly with \mathbf{k} near the Γ -point ($\mathbf{k} = 0$). We remark that Fig. 1 is obtained in a situation where J is larger than the other energy scales so that the electron spin direction is essentially parallel or anti-parallel to \mathbf{n} . Then the behavior of the energy bands in Fig. 1 can be summarized as the energy shift caused by the Rashba interaction $(\boldsymbol{\sigma} \times \mathbf{k}) \cdot \hat{z}$ in the presence of H_{ex} , demonstrating that the phenomenological Hamiltonian \mathcal{H} [Eq. (1)] can indeed be derived from the microscopic one, H_{TB} . This dependence of the energy bands on the \mathbf{n} direction has been utilized in the experiment [19] to verify the Rashba interaction at Gd surfaces.

The \mathbf{n} -dependent band shift noted in Fig. 1 vanishes when $\gamma = 0$. To capture the essential role of the ISB parameter in establishing the Rashba interaction we focus on $H_{\text{ISB}} = \sum_{\mathbf{k}} H_{\text{ISB}}(\mathbf{k})$, written in momentum space through $\mathbf{C}_{\mathbf{k},\sigma} = N^{-1/2} \sum_i e^{i\mathbf{k} \cdot \mathbf{r}_i} \mathbf{C}_{i,\sigma}$ [N =number of atomic sites]. Near the Γ -point we have $H_{\text{ISB}}(\mathbf{k}) = -2\gamma a_L \sum_{\sigma} \mathbf{C}_{\mathbf{k},\sigma}^\dagger (\mathbf{L} \cdot \mathbf{k} \times \hat{z}) \mathbf{C}_{\mathbf{k},\sigma}$, where a_L is the lattice constant. Thus \mathbf{L} tends to align along the $\pm \mathbf{k} \times \hat{z}$ direction. We then combine this tendency with $H_{\text{SOI}} = \sum_{\mathbf{k}} H_{\text{SOI}}(\mathbf{k})$, where $H_{\text{SOI}}(\mathbf{k}) = \lambda_{\text{so}} \sum_{\sigma,\sigma'} \mathbf{C}_{\mathbf{k},\sigma}^\dagger [\mathbf{L} \cdot (\boldsymbol{\sigma})_{\sigma,\sigma'}] \mathbf{C}_{\mathbf{k},\sigma'}$. Roughly speaking, the

combined effect of $H_{\text{ISB}}(\mathbf{k})$ and $H_{\text{SOI}}(\mathbf{k})$ is to replace \mathbf{L} in $H_{\text{SOI}}(\mathbf{k})$ by $\mathbf{k} \times \hat{z}$, producing the Rashba interaction proportional to $(\mathbf{k} \times \hat{z}) \cdot \boldsymbol{\sigma}$.

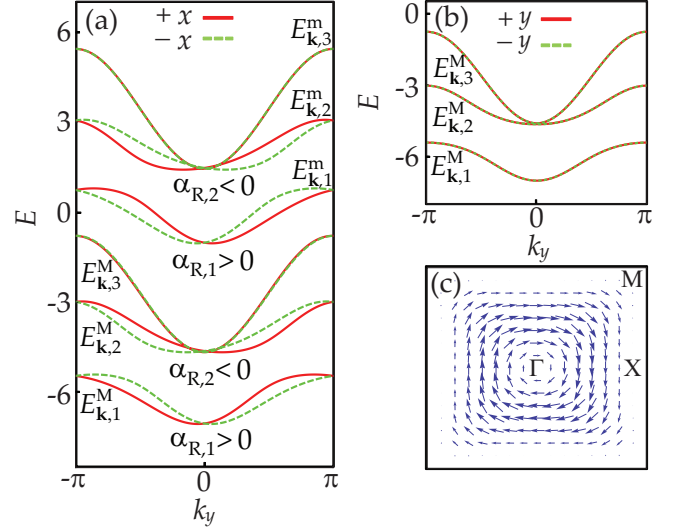


FIG. 1: (color online) (a) Energy bands for the tight-binding Hamiltonian H_{TB} with $(t_1, t_2, \gamma, \lambda_{\text{so}}, J) = (1, 0.2, 0.5, 0.5, 3.0)$. Red solid and green dashed lines are obtained for the unit magnetization vector \mathbf{n} directed along $+\hat{x}$ and $-\hat{x}$ directions, respectively. Majority (M) and minority (m) spin bands are labeled with superscripts. Signs of the Rashba parameters for the bands are indicated. The band $a = 3$ shows no Rashba effect as indicated by the absence of band shift. Energy dispersion along the k_y direction are shown. (b) No discernible difference in the band structure occurs along the k_y direction for magnetization \mathbf{n} directed along $+\hat{y}$ and $-\hat{y}$ directions. (c) Chiral OAM pattern for $a = 1$ majority band with $\lambda_{\text{so}} = 0$. Other parameters are the same as in (a).

This heuristic argument can be verified by a perturbation calculation. In the absence of H_{SOI} the bands separate into three majority ($\boldsymbol{\sigma} \parallel \mathbf{n}$) and three minority ($\boldsymbol{\sigma} \parallel -\mathbf{n}$) eigenstates $|\mathbf{k}, a\rangle \otimes |\boldsymbol{\sigma} \cdot \mathbf{n} = \pm\rangle$ ($a = 1, 2, 3$) of $H_{t_{2g}} + H_{\text{ISB}} + H_{\text{ex}}$. Within such band basis the spin-orbit Hamiltonian $H_{\text{SOI}}(\mathbf{k})$ becomes

$$H_{\text{SOI}}(\mathbf{k}) = \sum_{a=1}^3 \psi_{\mathbf{k},a}^\dagger \mathcal{H}_{\mathbf{k},a} \psi_{\mathbf{k},a} + \dots, \quad (4)$$

where $\psi_{\mathbf{k},a} = \begin{pmatrix} c_{\mathbf{k},a,+\mathbf{n}} \\ c_{\mathbf{k},a,-\mathbf{n}} \end{pmatrix}$ gives the spinor consisting of the majority ($\parallel +\mathbf{n}$) and the minority ($\parallel -\mathbf{n}$) a -band, and (\dots) gives the inter-band matrix elements which are ignored. The intra-band 2×2 matrix elements is obtained near the Γ -point as

$$\mathcal{H}_{\mathbf{k},1} = -\mathcal{H}_{\mathbf{k},2} = \alpha_{\text{R}}(\mathbf{k} \times \hat{z}) \cdot \boldsymbol{\sigma}, \quad \mathcal{H}_{\mathbf{k},3} = 0, \quad (5)$$

where $\alpha_{\text{R}} \equiv (\lambda_{\text{so}} a_L)(\gamma/t_1)$ is the Rashba parameter. Near the Γ -point the eigenstates also carry the chiral

OAM [15]

$$\langle \mathbf{k}, 1 | \mathbf{L} | \mathbf{k}, 1 \rangle = -\langle \mathbf{k}, 2 | \mathbf{L} | \mathbf{k}, 2 \rangle \simeq \frac{2\gamma}{t_1} \mathbf{k} \times \hat{z}, \quad (6)$$

whereas the eigenstates in the third band does not have OAM [15]. (Results over the full Brillouin zone are shown in Fig. 1(c) for $a = 1$ band.)

Putting all the pieces together and returning back to the real space, we arrive at the effective Hamiltonian truncated within each majority-minority spin-pair band a as $H_{\text{TB}} \approx \sum_a H_a$ with

$$H_a = \int d^2 \mathbf{r} \Psi_{\mathbf{r},a}^\dagger \left(\frac{\mathbf{p}^2}{2m_a^*} - J \boldsymbol{\sigma} \cdot \mathbf{n} + \alpha_{\text{R},a} (\boldsymbol{\sigma} \times \mathbf{p}) \cdot \hat{z} \right) \Psi_{\mathbf{r},a}, \quad (7)$$

where m_a^* is the effective mass of the band a . Because of the large value of J/α_{R} , the inter-band matrix elements in Eq. (4) only makes corrections which are second order in \mathbf{k} and are ignored in Eq. (7). Now the Rashba parameter becomes band-dependent, $\alpha_{\text{R},1} = \alpha_{\text{R}} = -\alpha_{\text{R},2}$ and even $\alpha_{\text{R},3} = 0$! Such non-trivial band dependence of the Rashba parameter cannot be understood from phenomenological consideration alone. As a result when the magnetization direction \mathbf{n} is reversed from $+\hat{x}$ to $-\hat{x}$, the corresponding shift in the band structure should occur in the opposite directions along the k_y -axis for $a = 1$ and $a = 2$ and not at all for $a = 3$, as is indeed the case; Fig. 1(a). For $\mathbf{n} = +\hat{y} \rightarrow -\hat{y}$ the shift in the k_y -direction is minimal; Fig. 1(b).

A few remarks are in order. Firstly, upon comparing Eq. (5) to Eq. (6) we deduce that the sign of the Rashba term in each majority-minority pair band a is correlated with the chirality of OAM for that band pair. The OAM non-carrying band $a = 3$, in turn, does not have the Rashba interaction. Both nonzero chiral OAM and Rashba interaction are consequences of multi-orbital character of the band and the inversion asymmetry. With the recently developed circular-dichroism angle-resolved photoemission technique one can independently probe the orbital chirality of the bands [20] and deduce the sign of the Rashba parameter for the specific band in question. Secondly, the connection between H_{ISB} in Eq. (2) and the combination $\mathbf{L} \cdot (\mathbf{k} \times \hat{z})$ is natural in view of symmetry, because the combination violates the inversion symmetry along z -axis and can thus arise generically when ISB occurs. In other models describing, for instance, p -electrons moving in 2D triangular (relevant for Bi) or square lattice, it can be shown that the additional hopping Hamiltonian [such as H_{ISB} in Eq. (2)] allowed by ISB is also proportional to the combination near the Γ -point. To be more strict, a more general Hamiltonian $\mathbf{L} \cdot [\mathbf{R}(\mathbf{k}) \times \hat{z}]$, where $\mathbf{R}(\mathbf{k})$ is an arbitrary odd function of \mathbf{k} consistent with the crystal symmetry, also violates the inversion symmetry. In fact, it can be verified that H_{ISB} in Eq. (2) is of this form with $\mathbf{R}(\mathbf{k}) = -2\gamma[\sin(k_x a_L)\hat{x} + \sin(k_y a_L)\hat{y}]$, which reduces to

$-2\gamma a_L \mathbf{k}$ near the Γ -point. Note that $\mathbf{R}(\mathbf{k}) \times \hat{z}$ explains the OAM pattern in the entire Brillouin zone in Fig. 1(c). Thirdly, although the derivation leading to Eq. (7) was done for small SOI, one can equally well solve the large-SOI limit and obtain the same Hamiltonian as Eq. (7) in the total spin $J = 1/2$ basis with $\alpha_{\text{R}} = \gamma a_L$ [15].

Band-to-band variations of $\alpha_{\text{R},a}$ imply that experimentally determined Rashba parameter [6] will be an average of $\alpha_{\text{R},a}$ in some sense. To clarify the nature of the averaging, we derive the Rashba-induced adiabatic STT [3] from our approach. To this end we now regard \mathbf{n} in Eq. (7) as position-dependent and introduce a \mathbf{r} -dependent SU(2) rotation of the operator $\Psi_{\mathbf{r}} = U_{\mathbf{r}} \psi_{\mathbf{r}}$ to adjust the spin of the conduction electron to localized spin, $U_{\mathbf{r}}^\dagger (\boldsymbol{\sigma} \cdot \mathbf{n}) U_{\mathbf{r}} = \sigma_z$ [21]. We focus on effects of one particular majority-minority band pair (subscript a is omitted) and return to the multiple-band case later. Approximating the emerging SU(2) gauge potential $-iU_{\mathbf{r}}^\dagger \partial_\mu U_{\mathbf{r}}$ by their diagonal components, $-iU_{\mathbf{r}}^\dagger \partial_\mu U_{\mathbf{r}} \simeq a_\mu \sigma_z$ [21], one arrives at the effective action \mathcal{S} , including the Berry phase action for spin \mathbf{n} and the spin Hamiltonian $H_{\mathbf{n}}$, as (I =spin size)

$$\begin{aligned} \mathcal{S} = & -2Ia_L^{-2} \int dt d^2 \mathbf{r} a_0 - \int dt H_{\mathbf{n}} \\ & + \int dt d^2 \mathbf{r} \psi_{\mathbf{r}}^\dagger [i\partial_t - a_0 \sigma_z] \psi_{\mathbf{r}} \\ & - \int dt d^2 \mathbf{r} \psi_{\mathbf{r}}^\dagger \left(\frac{[\mathbf{p} + \mathbf{a} \sigma_z]^2}{2m} - J \sigma_z \right) \psi_{\mathbf{r}} \\ & - \int dt d^2 \mathbf{r} \psi_{\mathbf{r}}^\dagger (\alpha_{\text{R}} (\mathbf{n} \times [\mathbf{p} \sigma_z + \mathbf{a}]) \cdot \hat{z}) \psi_{\mathbf{r}}. \quad (8) \end{aligned}$$

Landau-Lifshitz equation of motion for \mathbf{n} follows straightforwardly,

$$\begin{aligned} (Ia_L^{-2} + \rho^s) \partial_t \mathbf{n} + \mathbf{n} \times \frac{\delta H_{\mathbf{n}}}{\delta \mathbf{n}} \\ + (\mathbf{j}^s \cdot \nabla) \mathbf{n} + 2m\alpha_{\text{R}} \mathbf{n} \times (\mathbf{j}^s \times \hat{z}) = 0. \quad (9) \end{aligned}$$

The spin density takes on the usual form $\rho^s = \psi^\dagger \sigma_z \psi$, while the spin current is modified,

$$\mathbf{j}^s = \frac{1}{2m} (\psi^\dagger \sigma_z [\mathbf{p} \psi] - [\mathbf{p} \psi^\dagger] \sigma_z \psi) + \left(\frac{\mathbf{a}}{m} + \alpha_{\text{R}} \hat{z} \times \mathbf{n} \right) \psi^\dagger \psi, \quad (10)$$

due to the Rashba interaction. The last term on the l.h.s. of Eq. (9) is the adiabatic Rashba-induced STT discussed in Refs. [2-4]

For multiple bands crossing the Fermi level, the terms involving the spin current in the above equation are generalized to (restoring band index a)

$$\mathbf{j}^s \rightarrow \sum_a \mathbf{j}_a^s \equiv \mathbf{J}^s, \quad \alpha_{\text{R}} \mathbf{j}^s \rightarrow \sum_a \alpha_{\text{R},a} \mathbf{j}_a^s. \quad (11)$$

In light of the experimental condition which can only access the total current, \mathbf{J}^s , it becomes evident that the

experimentally measured α_R is the effective Rashba parameter $\alpha_{R,\text{eff}}$ defined as

$$\sum_a \alpha_{R,a} \mathbf{j}_a^s \equiv \alpha_{R,\text{eff}} \mathbf{J}^s. \quad (12)$$

Due to the band-to-band fluctuation of $\alpha_{R,a}$, $\alpha_{R,\text{eff}}$ is a sensitive function of the band structure and the position of the chemical potential. Rashba-induced non-adiabatic STT discovered recently [7, 8] cannot be derived without further including impurity terms in the effective action.

So far our discussion has implicitly assumed magnetic band which itself is subject to ISB γ and atomic spin-orbit coupling λ_{so} . In conventional 3d ferromagnets, an estimate of the Rashba parameter $\alpha_R \sim (\lambda_{\text{so}} a_L)(\gamma/t_1)$ yields at most 0.1 eVÅ since $\lambda_{\text{so}} \ll 100\text{meV}$ typical of 3d transition metals. In contrast, experimental values in the range of 1-2 eVÅ has been reported in 3d magnetic thin films covered with heavy-element layer [6], which suggests that mixing of atomic orbitals could result in hybridized bands with both strong magnetism and large Rashba interaction [22]. In non-magnetic systems, the enhancement of α_R through alloying has been reported [23].

The idea is readily confirmed by the first-principles calculation with, for example, one Co layer and three Pt layers forming a heterostructure where the inversion symmetry is naturally broken [24]. Isolating the eight bands around the Fermi level, band structures are calculated with the spin quantization axis constrained along $+\hat{x}$ and $-\hat{x}$ directions, respectively. The energy dispersion measured along the k_y -direction for the two cases are plotted in Fig. 2(a). The two bands at the top of the figure are nearly non-magnetic and experience little Rashba shift in response to the reversal of spin axis. For the remaining six bands which are magnetic, we deduce significant Rashba parameters $|\alpha_R| = 1 - 2\text{eVÅ}$ from the band shifts, in excellent quantitative agreement with recent experimental values [6]. Composition analysis revealed substantial fraction of both Co and Pt atoms for all the bands in support of the existence of new hybridized bands with both Rashba and magnetic characters. Similar to Fig. 1, the Rashba parameter is heavily band-specific [Fig. 2(a)]. In comparison a single magnetic Co layer yields almost no band shift as seen in Fig. 2(b). Even imposing perpendicular electric field of 1 eV/Å failed to improve the Rashba effect for the Co monolayer. As another comparison we carried out band structure calculations with one Co layer sandwiched between two Pt layers on either side to ensure inversion symmetry. Here we again find almost no Rashba shift of the band. It can be concluded, then, that twofold conditions are to be fulfilled for realizing magnetic bands with large Rashba coupling. One is the hybridization of magnetic and non-magnetic heavy atom orbitals to ensure the effective mixing of magnetism and spin-orbit interaction. The second is the inversion symmetry breaking such as available at surfaces and interfaces to ensure that

Rashba-type interaction becomes symmetry-allowed.

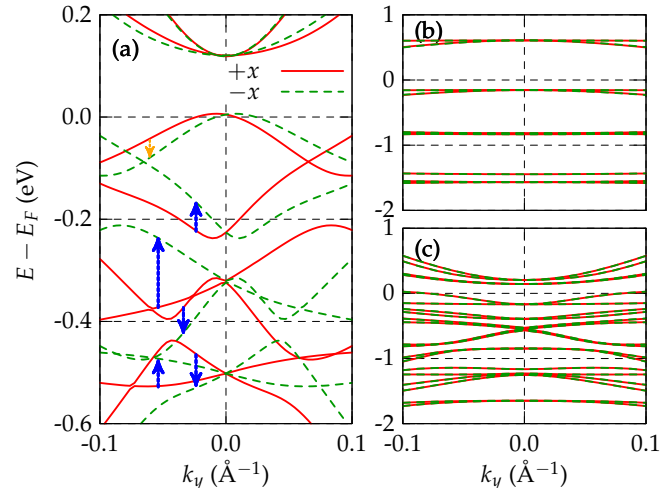


FIG. 2: (color online) (a) Band structure of 1Co-3Pt layers with the magnetization forced along $+\hat{x}$ (red full curves) and $-\hat{x}$ (green dashed curves) directions. Vertical arrows connect bands related by Rashba shift. The band associated with orange arrow is minority band while others with blue arrows are majority bands. Upward (downward) arrows imply positive (negative) Rashba parameter. The shift direction is reversed for the minority band. (b) 1Co layer. (c) 2Pt-1Co-2Pt layer. There is little Rashba shift observed in (b) and (c) between the two magnetization directions.

Essential aspects of the mixing can be understood by analysis of the tight-binding Hamiltonian, $H = H^{\text{NM}} + H^{\text{M}} + H^{\text{NM-M}}$, consisting of heavy non-magnetic (NM) bands with Rashba interaction, light magnetic (M) band, and their coupling (NM-M), respectively. Through the coupling, each Hamiltonian H_a in the non-magnetic Rashba band acquires a second-order correction in the hybridization parameter t_a between non-magnetic a -band and the magnetic band,

$$H_a \simeq \sum_{\mathbf{k}} \psi_{\mathbf{k},a}^\dagger \left(\varepsilon_{\mathbf{k},a} + \alpha_{R,a} (\boldsymbol{\sigma} \times \mathbf{k}) \cdot \hat{z} - \frac{|t_a|^2}{(\varepsilon_{\mathbf{k},a} - \varepsilon_{\mathbf{k},\text{M}})^2} J \boldsymbol{\sigma} \cdot \mathbf{n} \right) \psi_{\mathbf{k},a}. \quad (13)$$

Correction to the magnetic band is

$$H^{\text{M}} \simeq \sum_{\mathbf{k}} \psi_{\mathbf{k},\text{M}}^\dagger \left(\varepsilon_{\mathbf{k},\text{M}} - J \boldsymbol{\sigma} \cdot \mathbf{n} + \sum_a \frac{|t_a|^2 \alpha_{R,a}}{(\varepsilon_{\mathbf{k},a} - \varepsilon_{\mathbf{k},\text{M}})^2} (\boldsymbol{\sigma} \times \mathbf{k}) \cdot \hat{z} \right) \psi_{\mathbf{k},\text{M}}. \quad (14)$$

Apart from some energy dependencies in the denominator, both Hamiltonians (13) and (14) have remarkable resemblance to the effective Hamiltonian previously derived, Eq. (7). Based on insights from these perturbative calculations we claim the bands shown in Fig. 2(a) are

at once magnetic and carry a substantial Rashba parameter by virtue of the heavy mixing of magnetic and non-magnetic orbitals. The magnetization dynamics of the hybridized bands is also governed by Eqs. (7) through (12).

The present investigation showed how magnetic bands with substantial Rashba interaction can arise in mixed magnetic and heavy-element structures. In contrast to standard “relativistic” picture of Rashba effect, multi-orbital nature and atomic hybridization are crucial factors in forming the enhanced Rashba magnetic band. Currently available experimental values of α_R are very much scattered [6, 12, 25] even for apparently similar magnetic layer structures. We speculate that the sensitive band dependence of the effective Rashba parameter as discussed in Eq. (12) may be partially responsible for this. Away from the Γ -point the simple linear- \mathbf{k} dependence of the Rashba interaction should be replaced by some odd nonlinear function of \mathbf{k} , which will modify the angular dependence of Rashba-induced STT as well.

H. J. H. is supported by NRF grant (No. 2010-0008529, 2011-0015631). H. W. L. is supported by NRF grant (No. 2010-0014109, 2011-0030789). Informative discussions with Changyoung Kim and Dongwook Go are acknowledged.

* Electronic address: hwl@postech.ac.kr

† Electronic address: hanjh@skku.edu

- [1] D. C. Ralph and M. D. Stiles, *J. Magn. Magn. Mater.* **320**, 1190 (2008); Arne Brataas, Andrew D. Kent, and Hideo Ohno, *Nat. Mat.* **11**, 372 (2012).
- [2] K. Obata and G. Tatara, *Phys. Rev. B* **77**, 214429 (2008).
- [3] A. Manchon and S. Zhang, *Phys. Rev. B* **78**, 212405 (2008); *ibid.* **79**, 094422 (2009).
- [4] A. Matos-Abiague and R. O. Rodríguez-Suárez, *Phys. Rev. B* **80**, 094424 (2009).
- [5] Y. A. Bychkov and E. I. Rashba, *JETP Lett.* **39**, 78 (1984).
- [6] Ioan Mihal Miron *et al.* *Nat. Mat.* **9**, 230 (2010); *Nat. Mat.* **10**, 419 (2011); *Nature* **476**, 189 (2011).
- [7] Xuhui Wang and Aurelien Manchon, *Phys. Rev. Lett.* **108**, 117201 (2012); Xuhui Wang and Aurelien Manchon, arXiv:1111.5466 (2011); D. A. Pesin, A. H. MacDonald, arXiv:1201.0990 (2012); E. van der Bijl and R. A. Duine, arXiv:1205.0653 (2012).
- [8] Kyoung-Whan Kim, Soo-Man Seo, Jisu Ryu, Kyung-Jin Lee, and Hyun-Woo Lee, *Phys. Rev. B* **85**, 180404(R) (2012).
- [9] Kyoung-Whan Kim, Jung-Hwan Moon, Kyung-Jin Lee, and Hyun-Woo Lee, *Phys. Rev. Lett.* **108**, 217202 (2012).
- [10] G.Y. Guo, S. Murakami, T.-W. Chen, and N. Nagaosa, *Phys. Rev. Lett.* **100**, 096401 (2008); T. Tanaka, H. Kontani, M. Naito, T. Naito, D. S. Hirashima, K. Yamada, and J. Inoue, *Phys. Rev. B* **77**, 165117 (2008).
- [11] Luqiao Liu, Chi-Feng Pai, Y. Li, H. W. Tseng, D. C. Ralph, R. A. Buhrman, *Science* **336**, 555 (2012).
- [12] U. H. Pi, K. W. Kim, J. Y. Bae, S. C. Lee, Y. J. Cho, K. W. Kim, and S. Seo, *Appl. Phys. Lett.* **97**, 162507 (2010).
- [13] S. LaShell, B. A. McDougall, and E. Jensen, *Phys. Rev. Lett.* **77**, 3419 (1996).
- [14] Seung Ryong Park, Choong H. Kim, Jaejun Yu, Jung Hoon Han, and Changyoung Kim, *Phys. Rev. Lett.* **107**, 156803 (2011).
- [15] Jin-Hong Park, Choong H. Kim, Jun-Won Rhim, and Jung Hoon Han, *Phys. Rev. B* **85**, 195401 (2012).
- [16] L. Petersen and P. Hedegård, *Surf. Sci.* **459**, 49 (2000).
- [17] Masaru Onoda and Naoto Nagaosa, *J. Phys. Soc. Jpn.* **71**, 19 (2002).
- [18] This Hamiltonian is also a model of anomalous Hall effect, as shown in Ref. 17.
- [19] O. Krupin, G. Bihlmayer, K. Starke, S. Gorovikov, J. E. Prieto, K. Dobrich, S. Blügel, and G. Kaindl, *Phys. Rev. B* **71**, 201403 (2005).
- [20] Beomyoung Kim, Choong H. Kim, Panjin Kim, Wonsig Jung, Yeongkwan Kim, Yoonyoung Koh, Masashi Arita, Kenya Shimada, Hirofumi Namatame, Masaki Taniguchi, Jaejun Yu, and Changyoung Kim, *Phys. Rev. B* **85**, 195402 (2012).
- [21] G. Tatara, H. Kohno, and J. Shibata, *Phys. Rep.* **468**, 213 (2008).
- [22] M.-T. Lina, C. C. Kuo, H. Y. Her, Y. E. Wu, J. S. Tsay, and C. S. Shern, *J. Vac. Sci. Technol. A* **17**, 3045 (1999).
- [23] Christian R. Ast, Jürgen Henk, Arthur Ernst, Luca Moreschini, Mihaela C. Falub, Daniela Pacile, Patrick Bruno, Klaus Kern, and Marco Grioni, *Phys. Rev. Lett.* **98**, 186807 (2007).
- [24] For the first-principles density functional theory (DFT) calculations, we used the Ceperley-Alder parametrization of the local spin density approximation (LSDA) and projector augmented wave (PAW) potentials with the Vienna Ab-initio Simulation Package (VASP)[26]. The spin-orbit coupling was included self-consistently in the non-collinear DFT formalism. The lattice constant of Co in the hcp structure $a_{Co} = 2.507\text{\AA}$ was assumed for both Co and Pt layers.
- [25] L. Q. Liu, O. J. Lee, T. D. Gudmundsen, D. C. Ralph, R. A. Buhrman, <http://arXiv.org/abs/1110.6846>.
- [26] G. Kresse and J. Furthmüller, *Phys. Rev. B*, **54**, 11169 (1996); *ibid.* **59**, 1758 (1999).